Electronic Supplementary Information for:

Core-shell graphene oxide-polymer hollow fibers as water filters with enhanced performance and selectivity

Contents:

1. Chemical structures of Target EOCs and Polyethersulfone-polyvinylpirrolidinone fibers

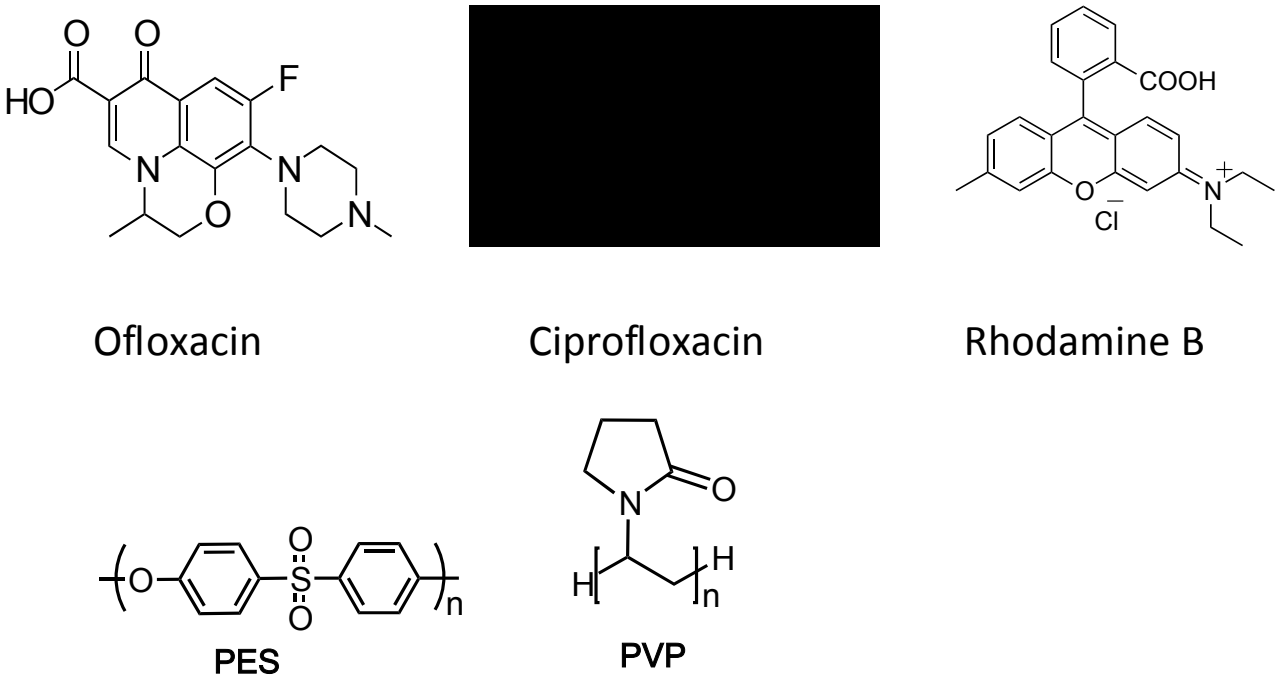

Figure S1. Molecular structure of the target EOCs and of the Versatile PES® polymeric components.

2. HF-GO cartridges preparation

GO powder (Abalonyx) was suspended in milliQ water (2mg/mL) and sonicated for 4 h. A volume of 5ml of GO suspension was filtered through PES cartridges (in-out or out-in configuration) then the cartridge was kept in oven at 80°C for 12 hs to give samples HF-GOo/i 1% (total weight of PES in the cartridge is about 700 mg). After cooling to room temperature, the filtration/fixation sequence was repeated a few times to give HF-GOo about 5% w/w (two further filtration/fixation cycles, for a total of three) and about 10% w/w in GO respectively (five further filtration/fixation cycles, for a total of six).

Cartridges nomenclature is:

HF-GO1e (out 1% GO),

HF-GO1i (in 1% GO),

HF-GO5e (out 5% GO),

HF-GO5i (in 5% GO),

HF-GO10e (out 10% GO),

HF-GO10i (in 10% GO).

3. Coating stability, filtered water potability

250 ml of tap water were filtered through a HF-GO5i cartridge (15ml/min).

Risultati analitici

Parametro *Metodo*	U.M.	Risultato	Incertezza	Limiti
* Torbidità APAT CNR IRSA 2110 Man 29 2003	NTU	< 0,02		
* Odore APAT CNR IRSA 2050 Man 29 2003		Inodore		
* Sapore APAT CNR IRSA 2080 Man 29 2003		Insapore		
* Colore APAT CNR IRSA 2020 Man 29 2003		Incolore		
pH APAT CNR IRSA 2060 Man 29 2003	upH	8,3	±0,4	6,5÷9,5
Conducibilità APAT CNR IRSA 2030 Man 29 2003	microS/cm	824	±62	< 2500
* Durezza totale APAT CNR IRSA 2040 Man 29 2003	°F	45,20	±6,78	15÷50
* Residuo fisso a 180 °C APAT CNR IRSA 2090 B Man 29 2003	mg/l	741,6		< 1500
* Carbonio organico totale (TOC) IRSA Q100 - 5030	mg/l	11		
* Azoto ammoniacale (come NH4+) APAT CNR IRSA 4030 A1 Man 29 2003	mg/l	< 0,1		
Cloruri APAT CNR IRSA 4020 Man 29 2003	mg/l	31,8	±2,9	
Solfati APAT CNR IRSA 4020 Man 29 2003	mg/l	85	±8	
Ferro (ICP-MS) EPA 6020B 2014	ug/l	24,0	±2,2	< 200
Alluminio (ICP-MS) EPA 6020B 2014	ug/l	72,4	±6,5	< 200
Manganese (ICP-MS) EPA 6020B 2014	ug/l	19,0	±1,7	< 50
* Sodio EPA 6010D 2018	mg/l	26,536	±2,388	< 200
* Cromo (ICP-MS) EPA 6020B 2014	ug/l	1,2		< 50
* Rame (ICP-MS) EPA 6020B 2014	ug/l	0,8		< 1,0
* Zinco (ICP-MS) EPA 6020B 2014	ug/l	1840,3		
* Mercurio (ICP-MS) EPA 6020B 2014	ug/l	< 0,1		< 1,0

Bologna lì: 10/10/2019

Il presente Rapporto di Prova si riferisce esclusivamente ai campioni sottoposti a prove ed è valido per tutti i casi previsti dalla legge come da R.D. 1/3/28 n. 842, art 16. Questo Rapporto di Prova non può essere riprodotto parzialmente salvo approvazione scritta del Laboratorio. Analisi eseguite presso la sede di Bologna

ACCREDIA

LAB N° 1051 L

Risultati analitici				
Parametro *Metodo*	**U.M.**	**Risultato**	**Incertezza**	**Limiti**
* Selenio (ICP-MS) EPA 6020B 2014	ug/l	< 0,1		< 10
* Vanadio (ICP-MS) EPA 6020B 2014	ug/l	0,6		< 50
* Arsenico (ICP-MS) EPA 6020B 2014	ug/l	0,1		< 10
* Cobalto (ICP-MS) EPA 6020B 2014	ug/l	0,29		
* Bario (ICP-MS) EPA 6020B 2014	ug/l	71,22		
* Berillio (ICP-MS) EPA 6020B 2014	ug/l	< 0,01		
Limiti: » D. Lgs. 31/01 Agg. D.M. 14/06/2017				

Table S1. Chemical potability parameters of filtered tap water (municipal Bologna network).

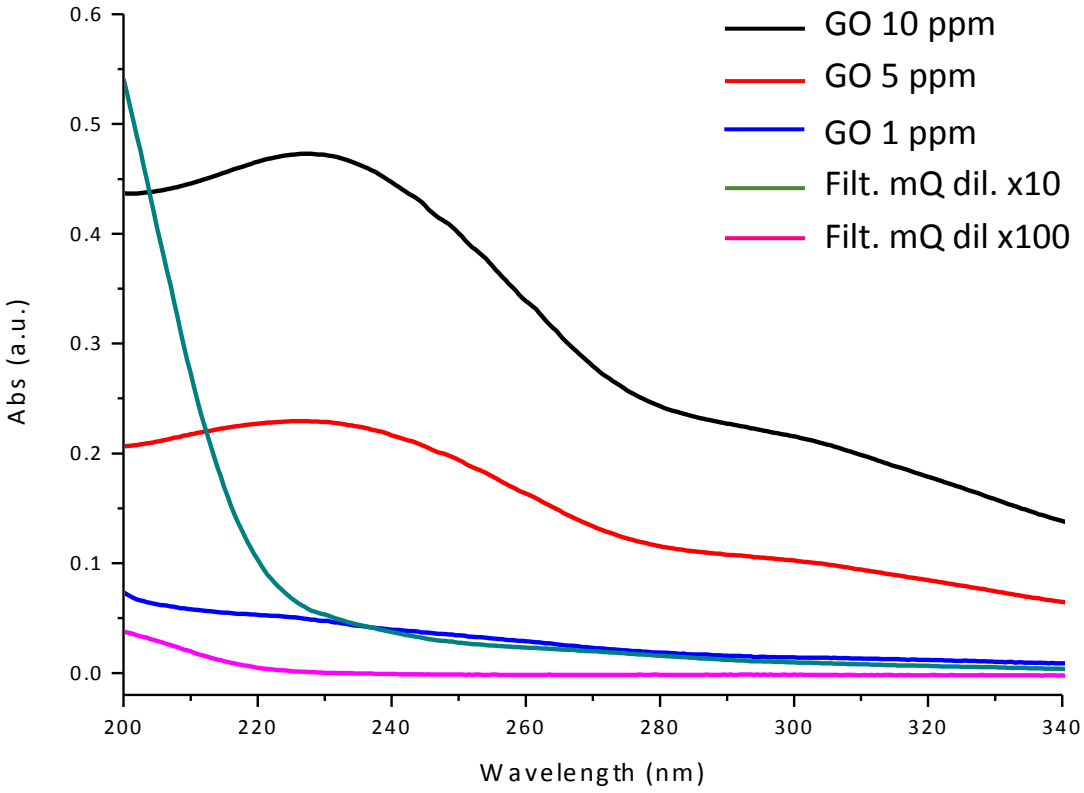

Figure S2. UV spectra of milliQ water filtered on HF-GO5e cartridge compared to calibrating solutions of GO.

4. Optical microscopy

HF-GO fibers were extracted from the cartridges and some cut samples (length about 1 cm) were put on a slide. Surface and section of the fibers were evaluated through optical microscopy under white light illumination with a Nikon Eclipse 80i microscope. Digital images were captured at 40x magnification with a Nikon camera (Digital Sight DS-5M) at a resolution of 1600 x 1200 pixels.

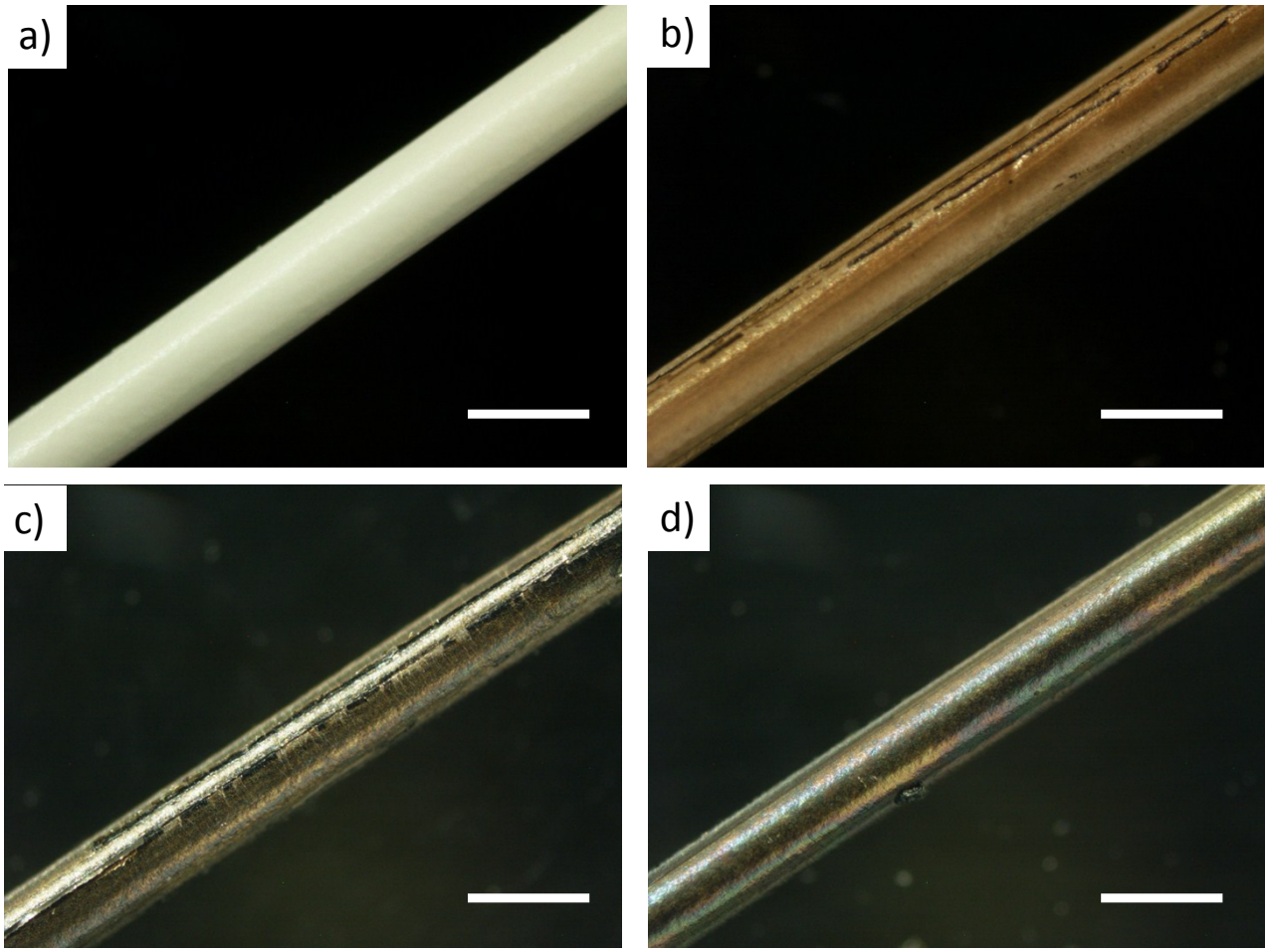

Figure S3. Optical microscopy of a) commercial PES (Versatile PES®), b) HF-GO1e, c) HF-GO5e and d) HF-GO10e. Bar size: 800 μm.

5. Scanning Electron Microscopy (SEM)

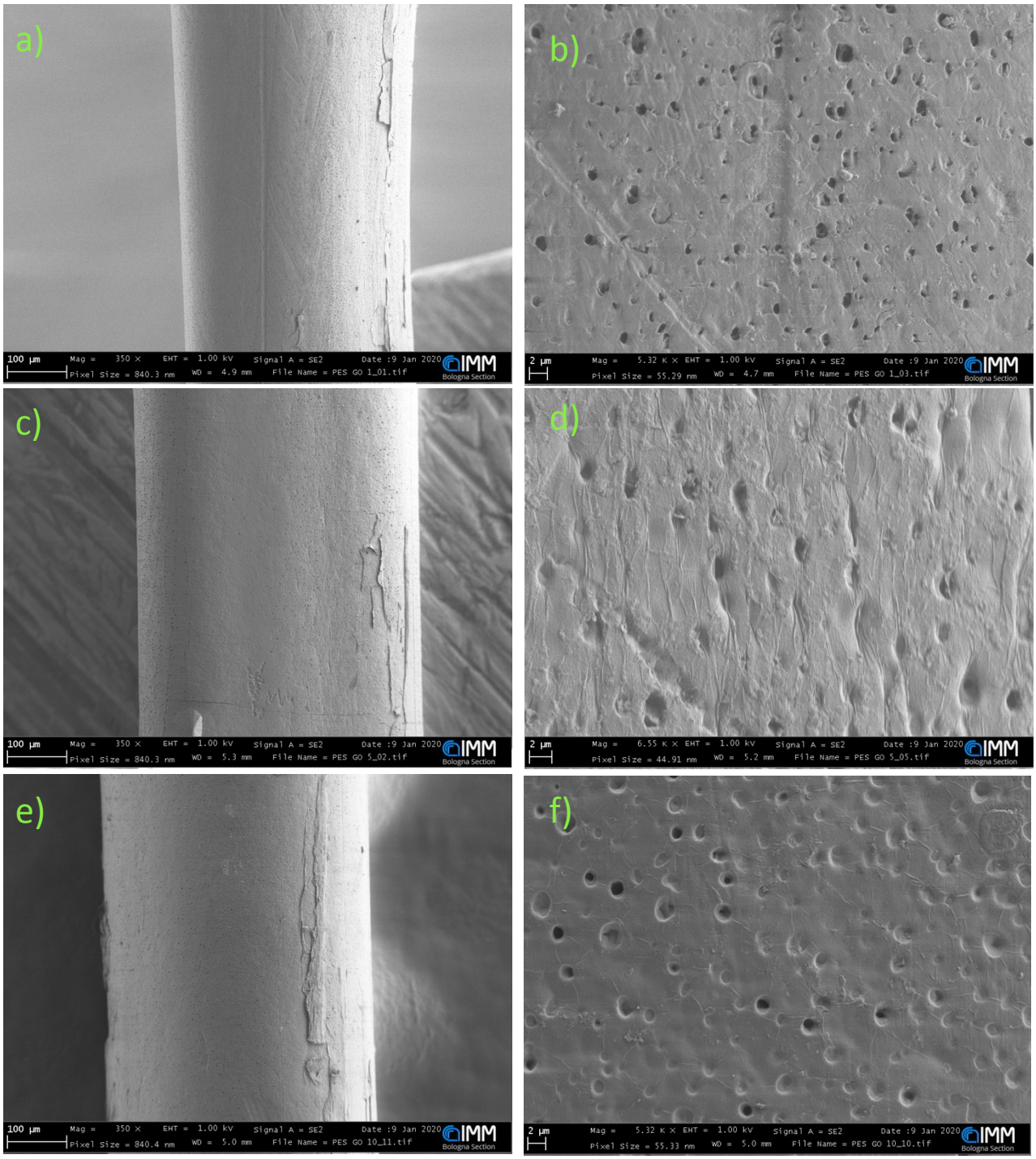

Figure S4. SEM images (at 1KV) of HF-GO1e (a,b)- HF-GO5e (c,d), HF-GO10e (e, f) at different magnification.

6. Micro-Raman

Micro-Raman spectra in the 1000–1800 cm^{-1} range were recorded in the unpolarized backscattering geometry through a Renishaw 1000 system (50x microscope objective) using the He-Ne excitation wavelength (632.8 nm).

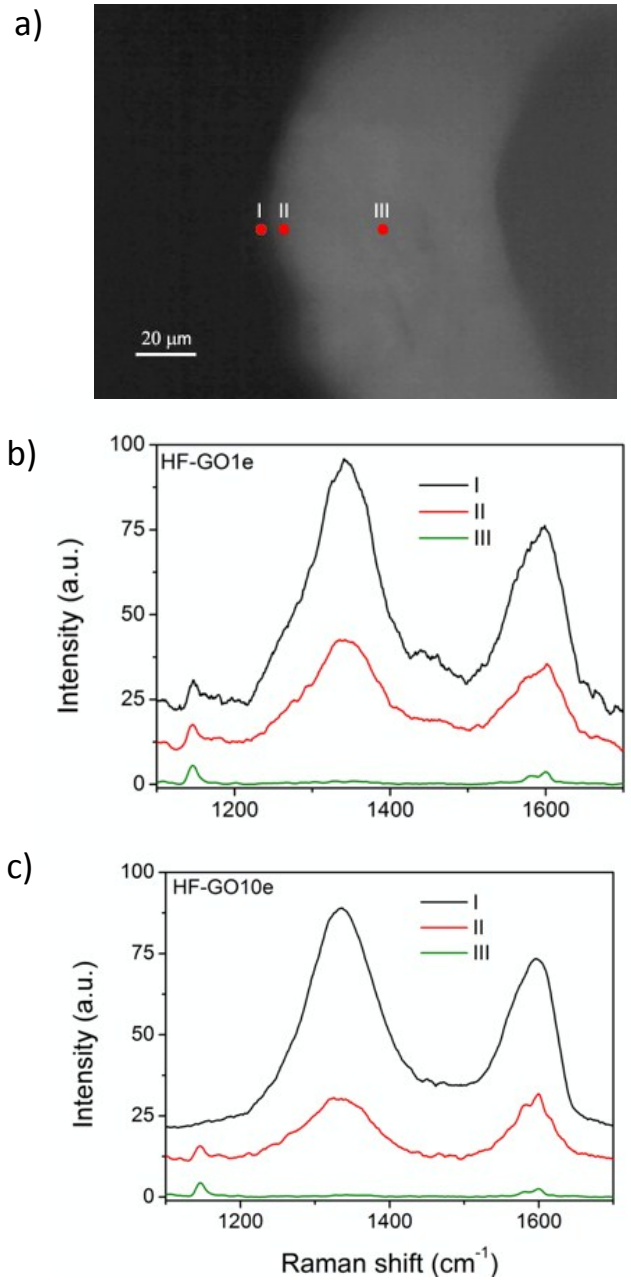

Figure S5. A) Optical microscope image of HF-GO10e cross section. Red dots indicate the Raman measurement points I) external wall; II) 5µm from the external wall; III) centre of the wall. B) Raman spectra of HF-GO1e collected, as indicated in figure S5, in different point of the HF-GO wall. The spectra have been renormalized with respect to the intensity of the PES Raman band at 1535 cm^{-1}. Raman PES peak at 1535 cm^{-1} is more intense in the uncoated inner region.

7. XRD analysis

The fibers were extracted from the cartridges and dried over night for 2h at 80°C before the analysis. The same treatment was performed on cartridges already used for filtering 250 mL of solution 5mg/L of oflox, ciproflox and RhB contaminants.

The analysis of cartridges already used for filtering 250 ml of solution 5mg/L of oflox, ciproflox and RhB contaminants,

PANalyticalX'Pert Pro X-ray diffractometer with nickel-filtered Cu Kα radiation and fast X'Celerator detector was used for recording the powder X-ray diffraction (XRD) patterns of all samples. Scherrer equation was used to calculate the crystal size (length of coherent domains):

$$L = (K*\lambda) / (\beta*\cos\theta) \quad \text{(S1)}$$

where *L* is a measure of the dimension of the particle in the direction perpendicular to the reflecting plane, λ is the X-ray wavelength, *K* is a constant (here, taken as 1), β is the peak width; and ϑ is the scattering angle. [1]

Table S2: crystal size (L) calculated from width of the *0 0 1* peak (FWHM) by Scherrer equation, and estimated number of GO layers (d=0.84 nm), rounded to closest unit.

	FWHM (°)	L (nm)	GO layers
HF-GO1e	1.22±0.05	7.3±0.3	9
HF-GO5e	1.43±0.05	6.2±0.2	7
HF-GO10e	1.75±0.05	5.1±0.1	6
GO	0.66±0.03	13.5±0.6	16

8. Water permeability test

Pumping osmotic ultrafiltered water at room temperature in a pressurized tank performed pure water permeability of the GO-coated cartridges. Filtration was performed in dead-end mode; pressure values were recorded at filter inlet with a pressure transducer and permeate was collected for 1 min and weighted. The effective membrane filtrating area of modules was 0,016 sqm. Three pressure values (between 100 and 300 mmHg) and three permeates were collected for each sample. Water permeability (or filtration coefficient) was then calculated as:

$$Kf = \frac{Quf\ (ml/min)}{\Delta P\ (mmHg)\ x\ A(sqm)} \quad \text{(S2)}$$

The average of the 3 values for each sample was reported as filtration coefficient.

9. Gas Permeability test

Air permeability tests were carried out on the complete set of membrane modules aiming at an indication of the resulting porous structure of the PES membrane system after coating by GO dispersions. Tests are carried out with dry compressed air at room temperature (20°C) and considering atmospheric pressure on the downstream side of the membrane. The measurements involved the determination of pressure drop given by the membrane systems by a differential manometer (resolution 0.1 mmH_2O), at constant flow rate obtained by a flow meter. The measured air permeance (or Transfer rate T.R.) of the coated membranes, or permeability of the GO layer only, provides an indication of the obtained structure, together with an estimation on the blocking effect given by the deposited GO layers. Interestingly, the results are not affected by any specific water/GO interaction, or even swelling effect on the GO stacking.

Gas permeance (T.R.) is obtained from the measured volumetric flux $I\&$ and the pressure drop:

$$\text{&}= I\& \frac{p}{RT} = T.R.\ \frac{\Delta p}{A} \quad \text{(S3)}$$

The results allowed the determination of the membrane permeance values reported in Table S3. As one can see, the transmembrane flux decreases significantly due to the presence of the GO coatings, and the more GO is deposited, the lower is the permeance. A large difference can be observed between membranes coated in the inner or in the external fiber layers, and it is very significant especially for lower concentration coatings; in particular, air permeance in HF-GO1i resulted to be 2 orders of magnitude higher than that in HF-GO1e, as a consequence of an incomplete coverage of the PES membrane fibers. The difference, however, disappears at the highest concentration, for which the air permeance becomes comparable.

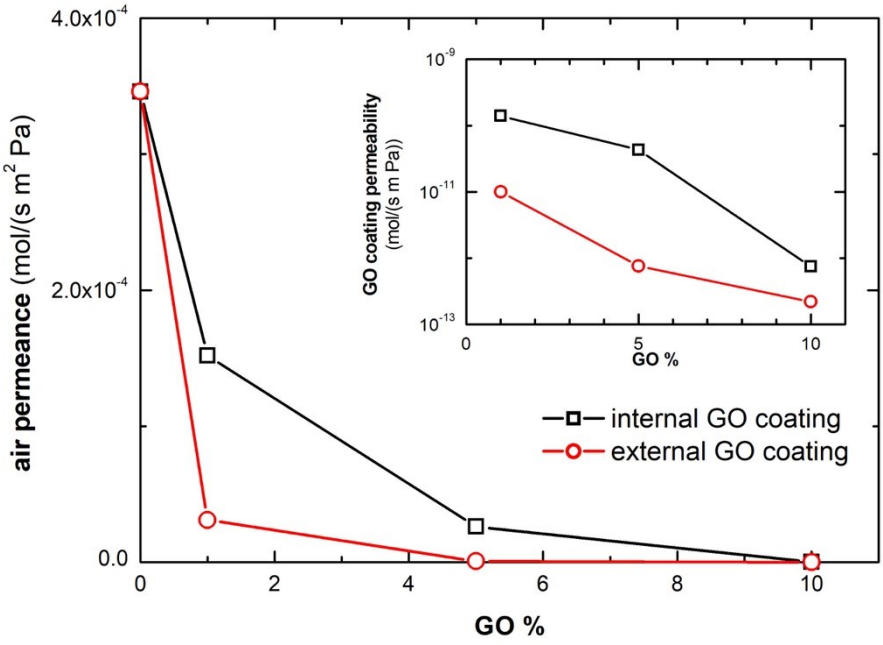

Figure S6. Air permeance in GO coated membranes.

Relevantly, based on the amount and the concentration of graphene oxide dispersion employed, it is possible to evaluate the average coverage of the membrane as mass of GO deposited per unit area. Furthermore, relying on literature data for stacked GO layers in graphene oxide paper, ρ_{GO} = 1.8 g/cm^3, [2] an effective thickness value for the coating layer has been determined and also included in Table 1.

Table S3. Air permeation properties in the coated membranes

	grammage [g/m^2]	eff. thick. [μm]	permeance [mol/(s m^2 Pa)]	GO permeability [mol/(m s Pa)]	D_{eff} [m^2/s]
neat PES	-	-	$3.5 \cdot 10^{-4}$	-	-
HF-GO1i	0.89	0.5	$1.5 \cdot 10^{-4}$	$1.4 \cdot 10^{-10}$	$3.4 \cdot 10^{-7}$
HF-GO5i	2.66	1.5	$2.6 \cdot 10^{-5}$	$4.3 \cdot 10^{-11}$	$1.1 \cdot 10^{-7}$
HF-GO10i	5.32	3.0	$2.4 \cdot 10^{-7}$	$7.5 \cdot 10^{-13}$	$1.8 \cdot 10^{-9}$
HF-GO1e	0.68	0.7	$3.1 \cdot 10^{-5}$	$1.1 \cdot 10^{-11}$	$2.5 \cdot 10^{-8}$
HF-GO5e	2.03	2.0	$8.6 \cdot 10^{-7}$	$7.6 \cdot 10^{-13}$	$1.9 \cdot 10^{-9}$
HF-GO10e	4.06	4.1	$1.2 \cdot 10^{-7}$	$2.2 \cdot 10^{-13}$	$5.3 \cdot 10^{-10}$

From simple resistance in series and relying on the estimated thickness, it is possible to evaluate the intrinsic (air) permeability of the GO coating only, assuming a uniform thickness (l_{GO}) of such coating on top of the microfiltration PES membrane.

$$\frac{1}{T.R.} = \frac{1}{T.R._0} + \frac{l_{GO}}{P_{GO}} \quad \text{(S4)}$$

Results obtained are also included in Table S3.

The resulting gas permeabilities can be interpreted from a phenomenological point of view, aiming to retrieve some information about the coating structure. Based on XRD measurements, the interlayer distance in the GO has been determined equal to d = 0.89 nm, which suggests a Knudsen diffusion mechanism in the GO coating (K_n > 10) to describe air molecules transport. The interlayer distance is expected to be the narrowest pore in the structure, and it is expected to be the controlling resistance. In these conditions, one can evaluate the diffusion coefficient from:

$$D_K = \frac{d}{3}\sqrt{\frac{8RT}{\pi M_i}} \quad \text{(S5)}$$

Therefore, Knudsen diffusivity in the slit results $D_K = 4.1 \cdot 10^{-7}$ m^2/s.

$$D_{eff} = P \cdot RT \quad \text{(S6)}$$

The calculated effective diffusion coefficient, included in Table S3, compared with the value of D_K in the GO slit, is very explicative in the understanding of the transport mechanism occurring in the GO coating, thus providing an idea about the coating structure.

The calculated diffusion coefficients at the lower concentration value (1%) are very large and not compatible with a Knudsen diffusion, and such effect has to be ascribed to an incomplete coverage of the hollow fibers, likely due to imperfect deposition in the small interstices. This is indeed apparent not only for HF-GO1i and HF-GO1e, but also for HF-GO5i. From simple calculations, one can obtain that about 44% of the surface of is not covered in the HF-GO1i membrane, such that a negligible barrier effect can be associated to that portion of the area. Indeed, the deposition of well-staked and overlapped GO layers leads to a significant barrier effect, definitely not comparable with the T.R. associated to a microporous membrane. Similarly, HF-GO1e and HF-GO5i can be considered as not fully covered, with about 9% and 5%, respectively, of uncovered surface.

The other membranes with a thicker coating (HF-GO5e, HF-GO10e and HF-GO10e) shows an effective diffusion coefficient significantly lower than D_K, and basically of the same order of magnitude, between 10^{-9} and $8 \cdot 10^{-10}$ m^2/s. That represents a clear indication that these structures are basically

equivalent (only thicker at the higher concentrations) and large by-passing holes are not present and there exists only a compact layer of GO sheets. The quite low value of D_{eff}/D_K, in the order of 10^{-3}, reveals that diffusing molecules are forced to travel around the GO sheets, thus leading to a tortuosity effect that depends on the in-plane distance between two near GO sheets and the intrinsic aspect ratio of the 2D materials.

10. BSA Filtration experiments and analytical method

Bovine serum albumin (BSA, 66KDa) was supplied by Sigma-Aldrich and used without any further purification. 10 mL of tap water solution of BSA (10 g/L) were loaded on a syringe and manually pushed into HF-GO cartridges with different GO content as well as a PES cartridge for comparison. The eluate was analysed by HPLC in order to evaluate BSA removal.

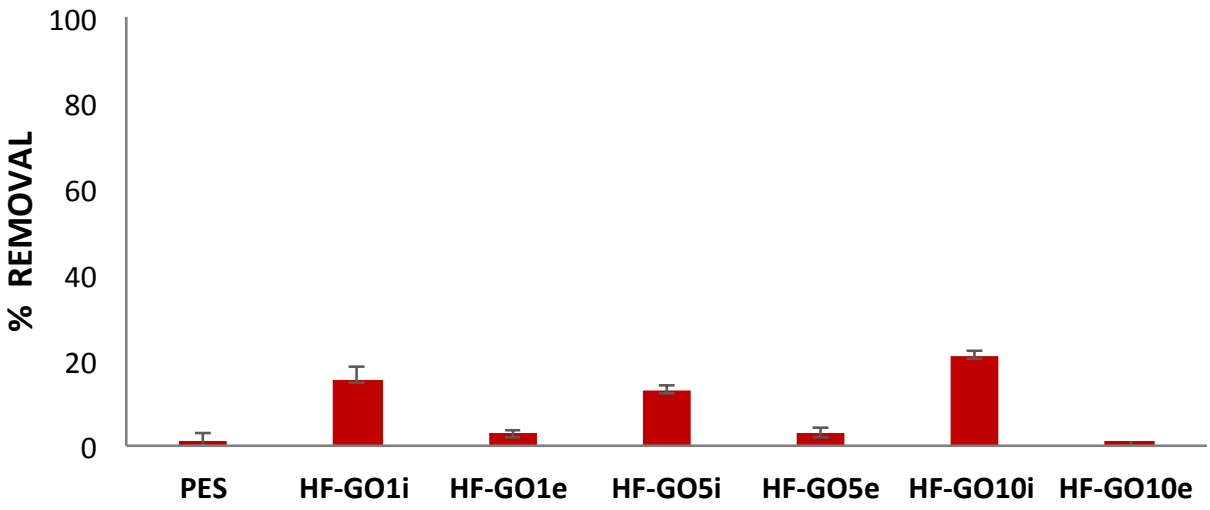

Figure S7. BSA removal efficiency by filtration on PES and HF-GO cartridges.

HPLC analyses were performed on a Dyonex Ultimate 3000 system equipped with a diode array detector. 0.5 mL samples were used as sources for the automated injection. LC-MS grade acetonitrile was purchased from Sigma-Aldrich in the highest available purity and were used without any further purification. Ultrapure water (resistivity 18.2 MΩ/cm at 25 °C) was produced in our laboratory by means of a Millipore Milli-Q system. The chromatographic separation was performed on a reverse phase Zorbax C8 column 4.6 x 150 mm, 5 μm, at flow rate of 1.0 mL/min, detection at λ 285 nm (details in table S4). In all experiments the removal of BSA was determined by comparison with that of the initial untreated solution. The results are expressed as the mean of three independent experiments ± SD.

Time (min)	H_2O (0.05% trifluoraocetic acid)	Acetonitrile	RT (min)
0	70	30	2.60
2	20	80	
3	20	80	
4	70	30	

Table S4. LC method for determination of BSA.

Filters were filled with a saline solution before the test. One sample of each type was assayed for in-out filtration (fig. S8a) and one for out-in filtration (fig. S8b). 10 ml of bovine plasma were loaded on a syringe and manually pushed into the filter. Three samples of filtrates were consecutively collected and the amount of TP and BSA was measured in the samples by BT1500 a clinical chemistry automatic analyzer.

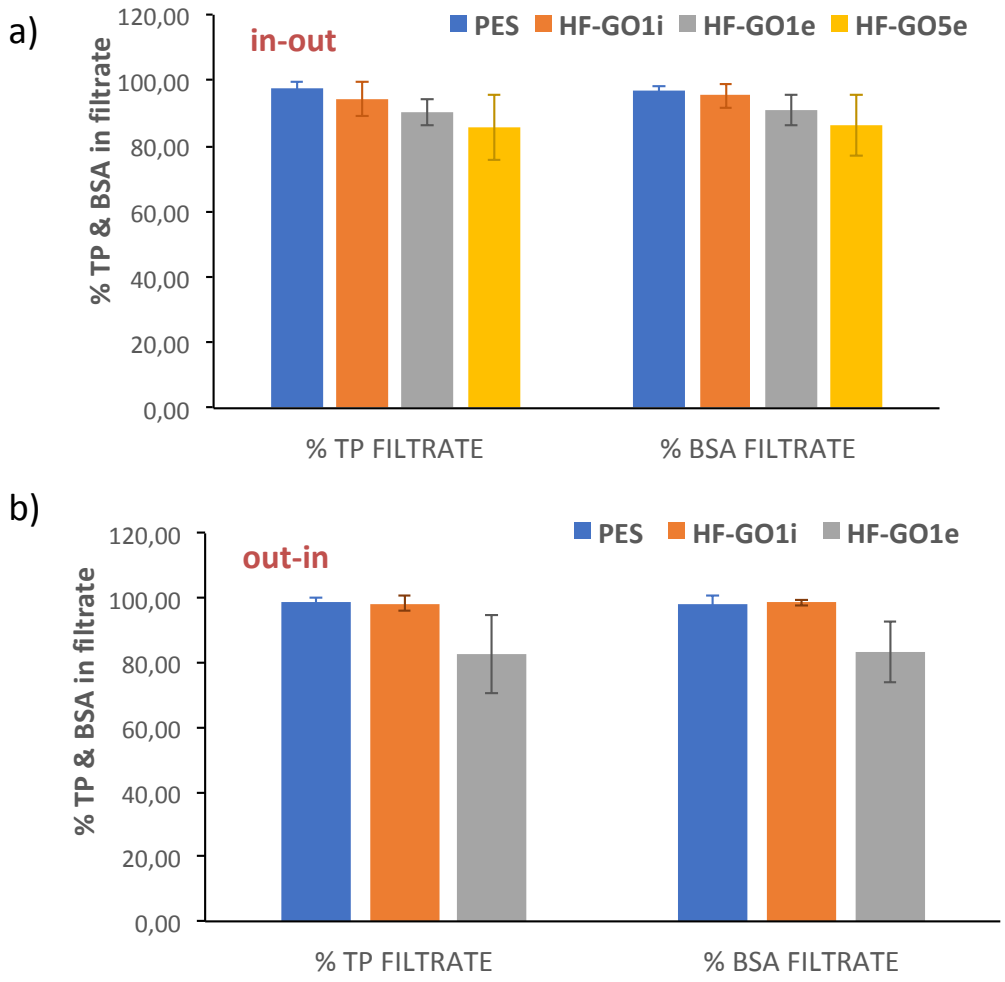

Figure S8. Filtration efficiency of total proteins (TP) and BSA (4 g/dl) for PES and HF-GO cartidges. Total proteins in plasma consist of albumin, globulines and fibrinogenes with a total concentration of 6-8 g/dL (60-80 g/L).

11. Nanoparticles filtration

Polystyrene Latex Particles Size 303 nm, (PS 303) conc. 0.1% w/v (Agar Scientific Ltd, UK), 0.1% = 1.000 ppm in water and Size 52 nm (PS 52), conc. 10% w/v (Magsphere Inc., USA), 10% = 100.000 ppm in water were used for determining the cut-off.

The nanoparticles were sonicated for 30 minutes and diluted in mQ water (1:10 PS 303, 1:100 PS52) and filtered through the cartridges. The concentration of NPs was determined by the absorbance intensity at 232 nm for the PS 303 and 213 nm for the PS 52, after a routine control of linearity of absorbance vs known concentration of nanoparticles.[3]

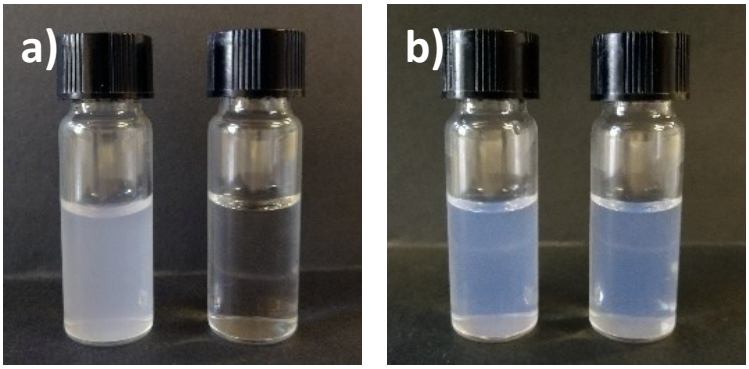

Figure S9. A) PS303 NPs and b) PS52 NPs suspensions before (left) and after (right) filtration on HF-GO1i cartridge.

12. Ofloxacin, Ciprofloxacin and Rhodamine B filtration experiments and analytical details

Ofloxacin (OFLOX), ciprofloxacin (Ciproflox), rhodamine B (RhB) were supplied by Sigma-Aldrich and used without any further purification. LC-MS grade acetonitrile was purchased from Sigma-Aldrich in the highest available purity and were used without any further purification. Ultrapure water (resistivity 18.2 MΩ/cm at 25 °C) was produced in our laboratory by means of a Millipore Milli-Q system.

A tap water solution of OFLOX, Ciproflox and Rh B in mixture at 5 mg/L concentration of each compound was prepared. Filtration experiments were performed on 250 mL of 5 mg/L solution fluxed at 15 mL/min flow. The fluxed solution was analyzed by HPLC in order to evaluate the removal efficiency for each EOC.

HPLC analyses were performed on a Dyonex Ultimate 3000 system equipped with a diode array detector. 0.5 mL samples were used as sources for the automated injection. The chromatographic separation was performed on a reverse phase Zorbax C8 column 4.6 x 150 mm, 5 μm, at flow rate of 1.0 mL/min, detection at λ of maximum UV absorption of the selected analyte (details in table S5-6). In all experiments the removal of analytes was determined by comparison with that of the initial untreated solution. The results are expressed as the mean of three independent experiments ± SD.

Time (min)	H_2O (0.05% TFA)	ACN
0	100	0
15	30	70
17	0	100
19	100	0

Table S5. LC method for determination of OFLOX, Ciproflox and RhB in mixture.

Compound	RT (min)	λ (nm)
OFLOX	12.30	285
Ciproflox	12.60	285
RhB	18.50	540

Table S6. Retention time and maximum absorption wavelenght of OFLOX, Ciproflox and RhB.

Figure S10 shows the removal efficiency of different chemicals analysed in present work, the removal efficiency depends from the interaction between GO and adsorbates. The Ciproflox has a better affinity with GO respect to the OFLOX and Rhodamine B. Figure S11 compares the removal efficiency of the different EOC studied for HF-GO1e, HF-GO5e and HF-GO1e filters. The removal is close to 90% only with 10% GO load.

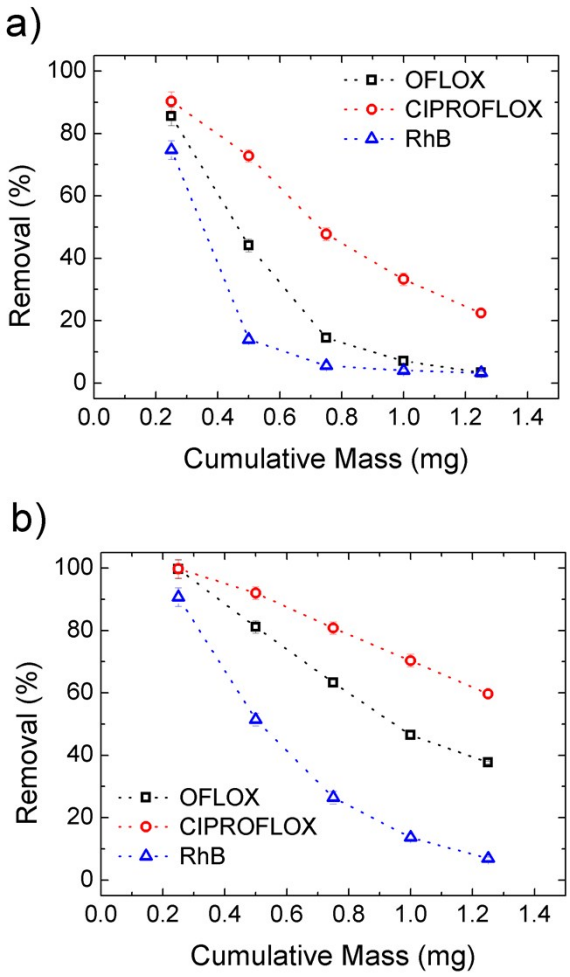

Figure S10. Removal efficiency for OFLOX, Ciproflox and RhB in case of a) HF-GO1i and b) HF-GO5i. Solution with fixed concentration (5 mg/L) and flow (15 mL/min).

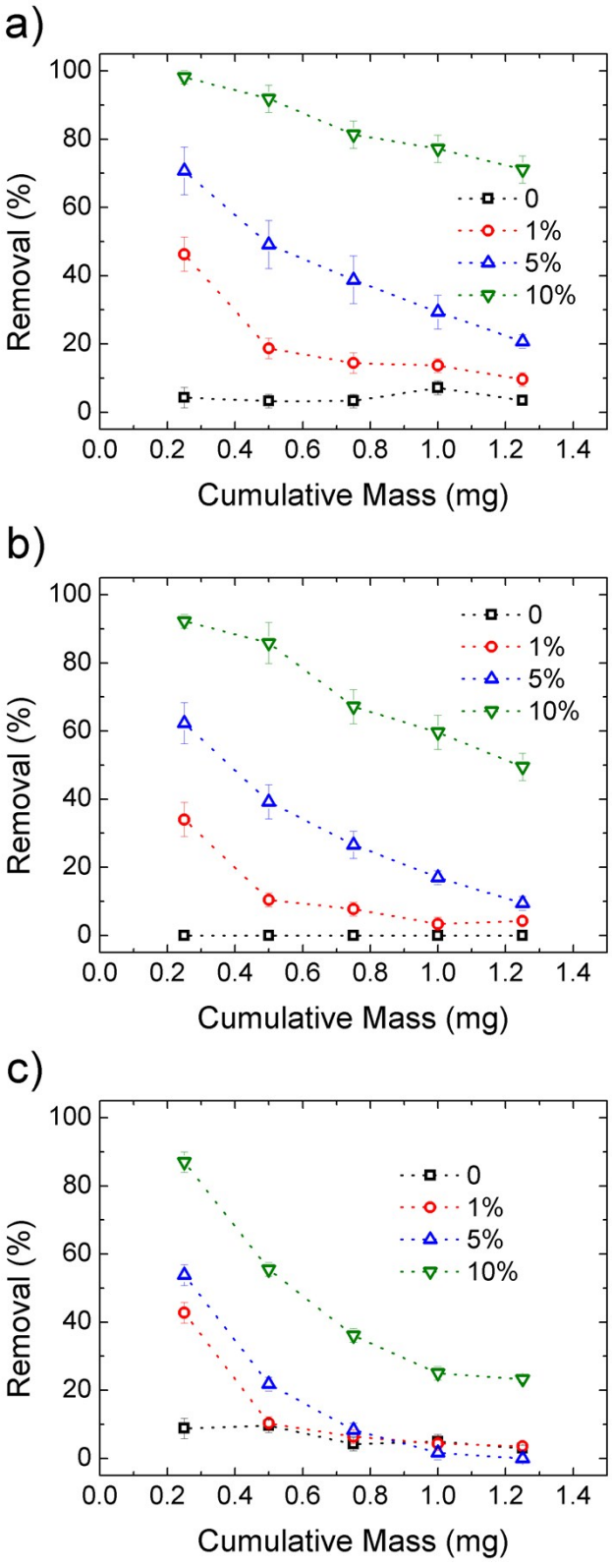

Figure S11. Removal efficiency for Ciproflox (a), OFLOX (b) and RhB (c) for PES and increasing GO loading in HF-GOe. The cumulative initial mass is obtained with fixed concentration (5 mg/L) and flow (15 mL/min).

The amount of EOC captured by GO (mg_{EOC}/g_{GO}) was determined for the sample HF-GO5i by selecting the EOC mass whit a removal close to 90%. The WWT-P usually operate at sub-ppb concentration of

EOC (C_{wwt}), and the overall efficiency can be intuitively expressed by the volume V of water filterable by a cartridge: $V= M_i/C_{wwt}$, where the M_i is the total mass of EOC fluxed through the filter. The volume of filterable water is reported in table S7. The efficiency of different active material should be compared by the ratio of the removed mass of EOC (M_R) over the mass of active material (M_{GO}), higher ratio corresponds to a more performing process. M_R/M_{GO} ratio has the same units of monolayer coverage mass (Q_m in mg/g) in Langmuir and BET isotherms, but is a completely different value, since it is measured out of thermodynamic equilibrium and at extremely low concentrations, when almost all the adsorption sites are available.

EOC	Removal %	M_i Initial (mg)	M_R removed mass (mg)	M_R/M_{GO} (mg/g)	C_{wwt} (ppb)	C_{wwt} (mg/L)	$V=M_i/C_{wwt}$ (L)
Ciproflox	91.6	0.5	0.458	15	0.2 *	$0.2\ 10^{-3}$	2500
OFLOX	81.8	0.5	0.409	14	0.4 *	$0.4\ 10^{-3}$	1250
RhB	89.1	0.25	0.2228	7	1	$1\ \ 10^{-3}$	250

Table S7. Values used for the estimation of filterable volume of water (V) by a single filter with a 90% c.a. of removal. *The C_{wwt} values were taken from ref. 4.

In order to compare the M_R/M_{GO} with other materials, like Powdered Activated Carbons (PAC), we used the data of ref. 4 on pilot WWT-P in Paris, that claims a removal efficiency close to 90% for c.a. 6 million L of water in 6 days with a material cost of 40 Kg of PAC. This means that 0.887 g of ciproflox was removed (C_{WWT}=0.172 ppb, M_i=1.02g) with a M_R/M_{PAC} of c.a. 20 µg/g.

13. Simultaneous filtration of proteins and OFLOX from water and bovine plasma matrixes

A tap water mixture solution of OFLOX and Bovine Serum Albumine (BSA) (50 mg/L and 10 g/L respectively) was prepared. 50 mL of OFLOX and BSA mixture were loaded on a syringe pump (1ml/min) into HF-GO cartridges as well as a PES cartridge for comparison. We consider only HF-GOi cartridges because of the better permeability values. The eluates were analysed by HPLC in order to evaluate OFLOX and BSA removal. HPLC analyses were performed on a Dyonex Ultimate 3000 system equipped with a diode array detector following the method previously described (table S4).
Typical chromatograms with estimated removals are shown in fig. S12.

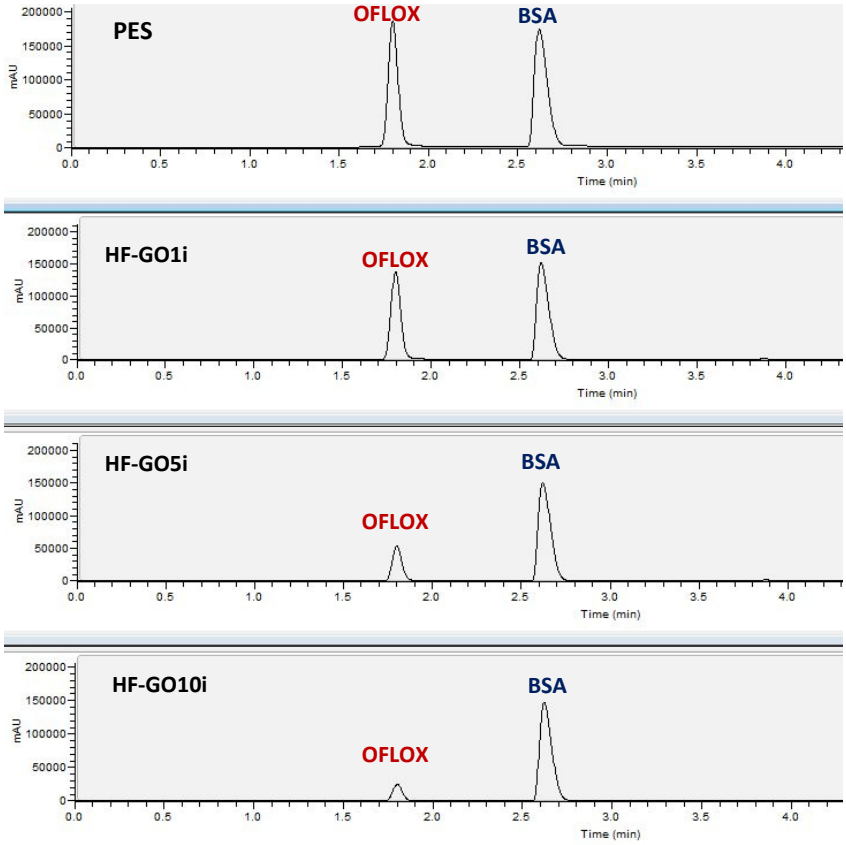

Figure S12. HPLC profile of OFLOX and BSA removal from water by filtration on PES and HF-GOi cartridges.

A similar experiment was performed in bovine plasma. Two stock solutions of OFLOX in water at 0.5 and 2 g/L were prepared. Bovine serum (9 mL) was spiked with 1 mL of the proper OFLOX stock solution to obtain 50 and 200 mg/L OFLOX final concentration. 10 mL of plasma/ofloxacin (50 and 200 mg/L) solution was loaded on a syringe and manually pushed into HF-GO1i. OFLOX was quantified by HPLC analysis following the method previously described (table S4). Prior to the HPLC analysis the eluate was treated as following described. 200 μL of the filtered solution was treated with equivalent amount of a tricloroacetic acid 5% and MeOH solution 3:1. After centrifugation (10000 rpm for 10 min) 3μL of NaOH 0.1% were added then the resulting solution was injected in HPLC. Figure S13 show the % removal of bovin plasma and total plasma proteins on HF-GO cartridges.

We used as case study HF-GO1i cartridges because of the higher permeability towards protein rich matrix like plasma.

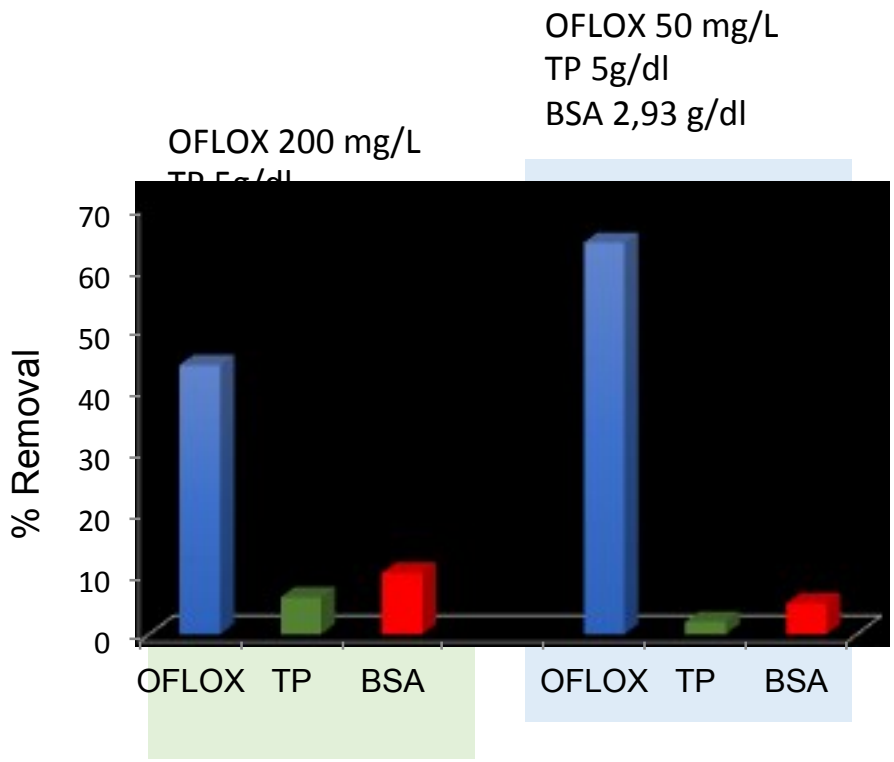

Figure S13. Simultaneous removal of BSA, TP and OFLOX from plasma by using HF-GO1i cartridges (one cartridge for each experiment, three repetitions). TP concentration in plasma is about 5 g/dl, BSA concentration is 2,93 g/dl.

14. Molecular modelling

To obtain structural information on the effect of ofloxacin intercalation on the spacing of GO layers, we carried out molecular mechanic studies using Gaussian 16.[4] UFF force field[5] was used to describe GO layers, water molecules and ofloxacin. Charges were assigned to all atoms using the QEq method.[6] Initial configurations of the GO nanoflakes were obtained by CSIRO Data Collection.[7] An initial spacing of 1 nm was used in the starting GO bilayer structure. Geometry optimizations were performed using Gaussian 16.[5]

15. References

[1] J.I. Langford, A.J.C. Wilson *J. Appl. Cryst.*, **1978**, *11*, 102-113.

[2] D. A. Dikin, S. Stankovich, E. J. Zimney, R. D. Piner, G. H. B. Dommett, G. Evmenenko, S. T. Nguyen, R. S. Ruoff, *Nature,* **2007,** *448*, 457–460.

[3] J. Shang, X. Gao, *Chem. Soc. Rev.,* **2014**, 43, 7267-7278.

[4] R. Mailler, J. Gasperi, Y. Coquet, S. Deshayes, S. Zedek, C. Cren-Oliv, N. Cartiser, V. Eudes, A. Bressy, E. Caupos, R. Moilleron, G. Chebbo, V. Rocher, *Water Research*, 2015, *72*, 315-330.

[5] Gaussian 16, Revision C.01, M. J. Frisch, G. W. Trucks, H. B. Schlegel, G. E. Scuseria, M. A. Robb, J. R. Cheeseman, G. Scalmani, V. Barone, G. A. Petersson, H. Nakatsuji, X. Li, M. Caricato, A. V. Marenich, J. Bloino, B. G. Janesko, R. Gomperts, B. Mennucci, H. P. Hratchian, J. V. Ortiz, A. F. Izmaylov, J. L. Sonnenberg, D. Williams-Young, F. Ding, F. Lipparini, F. Egidi, J. Goings, B. Peng, A. Petrone, T. Henderson, D. Ranasinghe, V. G. Zakrzewski, J. Gao, N. Rega, G. Zheng, W. Liang, M. Hada, M. Ehara, K. Toyota, R. Fukuda, J. Hasegawa, M. Ishida, T. Nakajima, Y. Honda, O. Kitao, H. Nakai, T. Vreven, K. Throssell, J. A. Montgomery, Jr., J. E. Peralta, F. Ogliaro, M. J. Bearpark, J. J. Heyd, E. N. Brothers, K. N. Kudin, V. N. Staroverov, T. A. Keith, R. Kobayashi, J. Normand, K. Raghavachari, A. P. Rendell, J. C. Burant, S. S. Iyengar, J. Tomasi, M. Cossi, J. M. Millam, M. Klene, C. Adamo, R. Cammi, J. W. Ochterski, R. L. Martin, K. Morokuma, O. Farkas, J. B. Foresman, and D. J. Fox, Gaussian, Inc., Wallingford CT, 2016.

[5] A. K. Rappé, C. J. Casewit, K. S. Colwell, W. A. G. III, W. M. Skiff, " *J. Am. Chem. Soc.* 1992, *114,* 10024-10035.

[6] A. K. Rappé, W. A. Goddard III, *J. Phys. Chem.* 1991, *95*, 3358-3363.

[7] A. Barnard, 2018 Graphene Oxide Structure Set. v1. CSIRO. Data Collection. https://doi.org/10.25919/5b91c8b150944